Subtle Chirality Effects of a D/L-Cysteine on the Intrinsic Acidity and Conformation of Isomeric Tripeptides ACA and A^{d}CA

Yuntao Zhang; Zachary Buen; Michael D. Browne; Yadwinder S. Mann; Jianhua Ren*

Department of Chemistry, University of the Pacific, 3601 Pacific Avenue, Stockton, CA 95211, USA

Running title: **Chirality Effects of a D/L-Cysteine on the Intrinsic Acidity**

* Corresponding Author: Jianhua Ren, PhD
Department of Chemistry
University of the Pacific
3601 Pacific Avenue
Stockton, CA 95211

Email: jren@pacific.edu
Phone: 209-946-2393
Fax: 209-946-2607

Abstract

Chirality effects on the intrinsic acidity of oligopeptides have been studied using a pair of stereoisomeric tripeptides containing two alanine (A) residues and either an L- or a D-cysteine, ACA and A^{d}CA, where the C-terminus is amidated. The gas-phase acidities were determined by mass spectrometry measurements. The extended kinetic method yielded the deprotonation enthalpy ($\Delta_{acid}H$) and the gas-phase acidity ($\Delta_{acid}G$) of ACA to be 328.0 and 322.7 kcal/mol (1372.4 and 1350.2 kJ/mol), and of A^{d}CA to be 327.8 and 322.4 kcal/mol (1371.5 and 1348.9 kJ/mol), respectively. Although the quantitative difference is small, the branching ratio bracketing experiments clearly indicate that A^{d}CA is a stronger gas-phase acid than ACA. Conformations were obtained via a step-wise conformational search, followed by geometry and frequency calculations at the B3LYP/6-311+G(d,p) level of theory. Theoretical gas-phase acidities are in good agreement with the experiments, which also suggests that A^{d}CA is a stronger gas-phase acid. The enhanced acidity of the D-cysteine containing peptide is likely due to the adoption of a unique bent conformation upon deprotonation at the thiol group, which enables more favorable hydrogen bonding interactions within the peptide ion. The findings imply that chirality change on a single amino acid residue may have a notable effect on the biochemical properties of peptides.

Keywords:

D-cysteine peptide, gas-phase acidity, deprotonation enthalpy, chirality effect, kinetic method, branching ratio

1. Introduction

Amino acids with one stereocenter can exist in both the Dextro (D) and Levo (L) configurations. An overwhelmingly vast majority of proteomic code seem to have preference for the L-amino acid residue in protein conglomerates. Although L-amino acids are preferentially selected by nature as the building blocks for proteins, D-amino acids (D-AA) have been found to be present in all living organisms, including humans, and fulfill specific biological functions.[1-3] For example, D-amino acids have been found to play regulatory roles in bacteria cell wall remodeling,[4] and in neurotransmission in the central nervous system in both animals and humans.[5, 6] Often times the presence of D-amino acids is associated with a variety of disorders and diseases ranging from ocular complications, arteriosclerosis, to Alzheimer's disease.[7-11] Since the isolation of the first D-amino acid containing peptide (DAACP), called dermorphin, from a frog skin in the early 1980s,[12] different DAACPs have been discovered from nervous tissue of various molluscs.[3, 13, 14] These peptides share an interesting common feature that only a single amino acid residue is in the D-form and the D-AA is most frequently located at the second position from the N-terminus.[15] Amidation at the C-terminus is another common feature of these DAACPs. The single D-AA is thought to be incorporated into the peptides through post-translational modifications, which converts the residue from the L-form to the D-form. The change of the configuration of the amino acid residue often modifies the biological activity of the peptides, and in many cases, enhances their biological functions.[13] The nature of the chirality change and the biochemistry of the DAACPs play remain largely unknown. To gain insight into the biochemistry of the DAACPs, it is important to study their intrinsic chemical properties as compared to peptides containing all L-amino acids.

Various mass spectrometry based analytical studies have been carried out by other researchers, including qualitative and quantitative identification of peptides containing D- and L-amino acids,[16-19] structural characterization of D-amino acid-containing peptides and peptide oligomers,[20-22] and identification and characterization of D-amino acid-containing neuropeptides,[13, 15, 23] Other researchers have also demonstrated that tripeptides displaced varied gas-phase acidities when the position of the acidic residue was changed.[24] An early study by Vaisar and co-workers shows that pentapeptide epimers displayed different proton affinities.[25] We have studied the intrinsic acid-base properties of a series of poly-alanine based oligopeptides containing an acidic or a basic residue as the acid-base probe.[26-30] These peptides are designed to reflect the structural features of the protein's active sites. For example, the cysteine-polyalanine series is based on the active site of the thioredixin family of enzymes that have an unusually acidic cysteine residue residing at the N-terminus of a helix motif.[31-35] The active site cysteine residue is readily deprotonated under physiological conditions and the resulting thiolate is considered one of the most powerful nucleophiles found in proteins.[36] A recent study by other researchers shows that incorporating a D-cysteine as opposed to an L-cysteine in a protein increased binding with metal ions.[37] Our studies have shown that in oligopeptides, a cysteine residue on the N-terminus displaces a significantly greater gas-phase acidity compare to the one on the C-terminus.[26-28]

In this study, we focus on using two stereoisomeric tripeptides as a model to examine how chirality change can alter the conformations and the gas-phase acidity, an intrinsic thermochemical property, of the peptides. As shown in Scheme 1, both peptides (ACA and A^{d}CA) have an alanine (A) residue on the N- and the C-terminus, and an L- or a D-cysteine (C or ^{d}C) in the middle, which is effectively the second position from the N-terminus. Both peptides

are amidated at the C-terminus, and therefore the thiol group of the side-chain of Cys is the only site for deprotonation in the gas-phase. In a previous study, we briefly measured the gas-phase acidity of ACA.[28] Because of the small structural difference between the two model peptides, the difference in the chemical properties could be subtle. Hence, it is important to carry out comparative experiments under the same conditions. In this work, ACA and A^{d}CA are characterized in detail with respect to their conformational features and gas-phase acidity.

Scheme 1. The stereoisomeric tri-peptides containing an L- and a D-cysteine

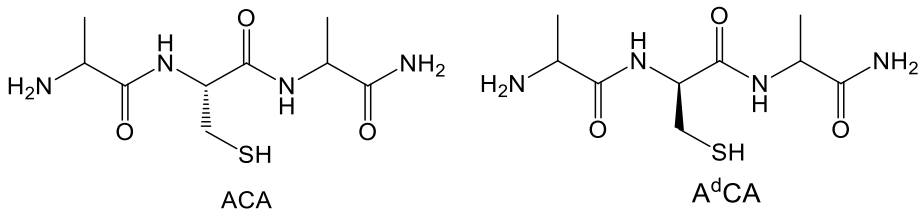

2. Experimental and Theoretical Methods

2.1 Peptide synthesis

The peptides used in this study were synthesized in our laboratory following the solid-phase peptide synthesis (SPPS) techniques.[38, 39] The detailed synthesis process has been described in our previous publications.[30] Briefly, the reactions were carried out in a semi-manual synthesis apparatus comprised of disposable synthesis vessels (Polypropylene reaction vessel, Torviq, Niles, MI) mounted onto a mechanical agitator (Model 75 Wrist-Action Shaker, Burrel Scientific, Pittsburgh, PA). Rink-amide resin was used as the solid support to yield the amide group at the C-terminus. Depending on the chirality of the Cys residue, either the Fmoc-

Cys(Trt)-OH (Chem-Impex International Inc.,Wood Dale, IL), or Fmoc-D-Cys(Trt)-OH (Sigma-Aldrich) was used for incorporating the Cys residue. Rink-amide resin, Fmoc-Ala, and other synthesis reagents were purchased from Chem-Impex International Inc., and were used without further purification. The synthesis reagents included O-Benzotriazole-N,N,N',N'-tetramethyl-uronium-hexafluoro-phosphate (HBTU), and 9-fold excess N,N-Diisopropylethylamine (DIPEA). The peptide was cleaved off the resin by using a cleavage cocktail (88% trifluoroacetic acid (TFA), 5% phenol, 5% H_2O, and 2% triisopropylsilane (TIPS)). The crude product was purified by recrystallization from a mixture of diether ether and hexane, and then dissolved in HPLC-grade water. After lyophilization twice, the resulting peptides were used for mass spectrometry experiments. Peptide sequence was confirmed by tandem mass spectrometry sequence analysis.

2.2 Mass spectrometry and parameters

Mass spectrometry measurements were performed using a Varian 320L (Agilent Technologies, Santa Clara, CA) triple quadrupole mass spectrometer coupled to an electrospray ionization (ESI) source. Data was acquired and recorded using the Varian MS Workstation software package (Version 6.9). All experiments were carried out in the negative ion mode. Compressed air (Fresno Oxygen, Fresno, CA) was used as the nebulizing gas with a pressure of 38.0 to 45.0 psi. Nitrogen (Ultra-High Purity, Air Products and Chemicals Inc.) was utilized as the drying gas with a pressure of 10.0 to 14.0 psi and a temperature of 160°C to 190 °C. The ESI needle voltage and the shield voltage remained at -4.5 kV and 600 V, respectively, throughout the experiments. The capillary voltage was around -40 to -45 V. The ion guide chamber

remained at about 1 mTorr and had a temperature of about 40 °C. Some experimental parameters (capillary voltage, nebulizer and drying gas pressures, and drying gas temperature) were further adjusted to maximize the precursor ion signal to at least 40 mV (instrument parameter). Ions generated were presumed to be thermalized within the ion guide chamber by multiple collisions with ~1 mTorr nitrogen gas prior to entry into the first quadrupole unit (Q1). Product ion analysis experiments were performed by selecting the ion of interest (the proton-bound dimer, based on the *m/z* value) in Q1 with a peak width of 1.0 to 1.2 (instrument parameter) depending on the ion intensity. The selected ions then entered into the quadrupole collision cell (Q2) where they were subjected to collision induced dissociation (CID) with argon gas. For most experiments, the argon gas pressure remained at 0.300 ± 0.020 mTorr. The collision energy ranged from 1.5 eV to 3.0 eV, in the center-of-mass frame. The center-of-mass energy (E_{cm}) was calculated using the equation $E_{cm}=E_{lab}[m/(M+m)]$, where E_{lab} is the laboratory frame collision energy, m is the mass of argon, and M is the mass of the precursor ion. The dissociation product ions were analyzed using the third quadrupole (Q3) with a peak width up to 1.2.

2.3 Branching ratio bracketing for gauging relative gas-phase acidity

For the purpose of examining the relative gas-phase acidity of the peptides, the CID branching ratio bracketing experiments were carried out. A series of reference acids with known gas-phase acidities were selected. The reference acids as well as the peptides were dissolved separately into a mixed solvent of MeOH:H_2O (1:1, v:v) to make stock solutions of about 10^{-3} M. A mixed solution of a peptide and a reference acid was diluted to about10^{-4} to 10^{-5} M and was introduced into the ion source to form a proton-bound dimer ion, $[pep•H•ref]^-$, where “pep” and “ref” represented the components of deprotonated peptide and reference acid, respectively. The

proton-bound dimer was isolated in Q1, fragmented in Q2 (the CID process), and analyzed in Q3. The CID experiments were carried out at 7 collision energies (E_{cm}) from 1.5 eV to 3.0 eV with 0.25 eV energy increments. At lower collision energies, the main fragment ions were the deprotonated peptide (pep^-) and the deprotonated reference acid (ref^-). At higher collision energies, secondary fragments occurred. The fragment ion intensities (I_{pep}^- and I_{ref}^-) were recorded using the selected reaction monitoring (SRM) mode continuously for 3 minutes. The dwell time during the SRM experiments for each selected product ion was 0.100 seconds with a total of forty separate scans for each product ion. Each experiment was replicated on three separate days and the data was averaged. Branching ratios, $ln[(I_{pep}^-)/(I_{ref}^-)]$, were obtained at all collision energies. Secondary fragment ions were linearly incorporated into the primary fragments to yield the data of I_{pep}^- and I_{ref}^-. Branching ratio plots were constructed by plotting $ln[(I_{pep}^-)/(I_{ref}^-)]$ against collision energy (E_{cm}).

2.4 Extended kinetic method for gas-phase acidity determination

The quantitative values of the gas-phase acidity of the peptides were determined using the extended kinetic method (EKM). The method was introduced by Cooks and coworkers and was refined by other researchers.[40-47] The gas-phase acidity is given by the equation, pepH → $pep^- + H^+$, which can be described with the thermodynamic values of gas-phase acidity $\Delta_{acid}G$, deprotonation enthalpy $\Delta_{acid}H$, and deprotonation entropy $\Delta_{acid}S$. The EKM procedure begins with generating and isolating the proton-bound dimer, $[pep•H•ref]^-$, in the ion source and Q1, respectively. The proton-bound dimer undergoes the CID process (in Q2) to produce corresponding fragment ions, pep^- and ref^- (detected in Q3). The CID experiments are carried out at multiple collision energies, and the branching ratios, $ln[(I_{pep}^-)/(I_{ref}^-)]$, are obtained. The

data are analyzed using the linear relationship described in eq. (1), where $\Delta_{acid}H_{pep}$ and $\Delta_{acid}H_{ref}$ are the deprotonation enthalpies of the peptide and the reference acid, respectively, $\Delta_{acid}H_{avg}$ is the average deprotonation enthalpy of the reference acids,[45, 46] and R is the ideal gas constant. In this equation, T_{eff} is the "effective temperature" of the activated proton-bound dimer.[48-52] The term $\Delta(\Delta_{acid}S)$ is the difference in deprotonation entropy between the peptide and the reference acid. The latter can be represented by the average deprotonation entropy of the reference acids, eq. (2), considering that the reference acids used are of similar structure and have similar deprotonation entropies.[26] The values of $\Delta_{acid}H_{pep}$ and $\Delta_{acid}S_{pep}$ are directly obtained from the EKM. Although the exact temperature of the gas-phase ions is unknown, the value of "effective" gas-phase acidity at 298 K, $\Delta_{acid}G_{pep}$, can be obtained from eq. (3).

$$ln\left(\frac{[I_{pep}^-]}{[I_{ref}^-]}\right) = \frac{\Delta_{acid}H_{ref} - \Delta_{acid}H_{avg}}{RT_{eff}} - \left[\frac{\Delta_{acid}H_{pep} - \Delta_{acid}H_{avg}}{RT_{eff}} - \frac{\Delta(\Delta_{acid}S)}{R}\right] \quad (1)$$

$$\Delta(\Delta_{acid}S) = \Delta_{acid}S_{pep} - \Delta_{acid}S_{ref} \approx \Delta_{acid}S_{pep} - \Delta_{acid}S_{avg} \quad (2)$$

$$\Delta_{acid}G_{pep} = \Delta_{acid}H_{pep} - T(\Delta_{acid}S_{pep}) \quad (3)$$

The data treatment involves constructing two linear thermo-kinetic plots by using eq. (1). First, a plot of $ln([I_{pep}^-]/[I_{ref}^-])$ against $\Delta_{acid}H_{ref} - \Delta_{acid}H_{avg}$ is generated, in which the slope represents $1/RT_{eff}$ and the y-intercept represents $Y = -[(\Delta_{acid}H_{pep} - \Delta_{acid}H_{avg})/RT_{eff} - \Delta(\Delta_{acid}S)/R]$. Next, a plot of Y (y-intercept) against $(1/RT_{eff})$ is made, in which the slope represents $-[(\Delta_{acid}H_{pep}$

$- \Delta_{acid}H_{avg}$] and the y-intercept represents $\Delta(\Delta_{acid}S)/R$, where $\Delta(\Delta_{acid}S) \approx \Delta_{acid}S_{pep} - \Delta_{acid}S_{avg}$. Since $\Delta_{acid}H_{avg}$ and $\Delta_{acid}S_{avg}$ are known, so $\Delta_{acid}H_{pep}$ and $\Delta_{acid}S_{pep}$ can be obtained.

The absolute uncertainty of $\Delta_{acid}H_{avg}$ (σ_{avg}) was calculated as the root sum square of the systematic error (σ_{cys}) and the random error (σ_{rand}), $\sigma_{avg} = \sqrt{[(\sigma_{cys})^2 + (\sigma_{rand})^2]}$. Assuming that N number of reference acids is used and each reference acid has an uncertainty of ±2.0 kcal mol^{-1}, thus, $\sigma_{cys} = \sqrt{2.0}$, $\sigma_{rand} = 2.0/\sqrt{N}$, and $\sigma_{avg} = \sqrt{[(\sqrt{2.0})^2 + (2.0/\sqrt{N})^2]}$. The uncertainty analysis was carried out through the linear regression for both of the thermo-kinetic plots using the ODRPACK program, which simultaneously calculates the uncertainties in both the x and the y directions.[53] In the first plot, a ±2.0 kcal mol^{-1} was used for the x-axis and an average of ±5% was used for the y-axis, which was based on the variations of the measured branching ratios over several days. The resulting uncertainties in the slope and the y-intercept were then inputted into the second plot, which yielded the corresponding uncertainties σ_x for the term $\Delta_{acid}H_{avg} - \Delta_{acid}H_{pep}$ and σ_y for the term $\Delta_{acid}S_{avg} - \Delta_{acid}S_{pep}$. The final uncertainties in $\Delta_{acid}H_{avg}$ and $\Delta_{acid}S_{avg}$ were given by $\sigma = \sqrt{(\sigma_{avg}^2 + \sigma_x^2)}$ and $\sigma = \sqrt{(\sigma_{avg}^2 + \sigma_y^2)}$, respectively.

The source of the absolute uncertainty is mainly due to the errors associated with the acidity scale if the reference acids used for the measurements. For peptide systems using the same or comparable reference acids, the absolute uncertainties in the relative gas-phase acidities between the peptide systems are largely canceled out. The relative uncertainties allow for the comparison of the subtle acidity changes among isomeric peptides. The relative uncertainties can be gauged by using the standard deviations of the acidity values measured in multiple days. An example is given in the result section.

The extended kinetic method has been shown to produce precise values of thermochemical properties for systems involving rigid molecules for which the entropic effects and the reverse activation barriers are minimized.[41] However, for systems involving structurally flexible analyte and reference compounds, entropic effects and reverse activation barriers could cause errors to the measured values of ion affinity.[54, 55] The issues have been discussed by other researchers in a series of papers.[46, 47, 49, 56] This problem could be reduced by carefully selecting reference compounds, employing as many references as possible, and measuring the branching ratios over a wide energy range.

2.5 Computational method

Computations were carried out by a conformational search at low levels of theory and followed by geometry and frequency calculations at a high level of theory. We employed two approaches to search for the most possible conformations of the neutral and the charged peptides. The first one is the "funneling-approach" which begins with generating a large number of conformations and gradually filters away high energy conformations. We have used this approach to calculate several small peptides systems.[30, 57] By using an ideal helical conformation as the input geometry, 100,000 possible conformations were sampled with the Merck Molecular Force Field (MMFF) implemented in Spartan'14 software package (Wavefunction, Irvine, CA).[58] The 100 lowest energy conformations were retained and were subjected to PM3 semi-empirical quantum level calculations for both geometry and frequency. The same set of conformations were further calculated for both geometry and frequency at the Hartree Fock (HF) level of theory with the 3-21G basis set to yield a better energy ladder. This step and additional calculations were carried out using the Gaussian 16' suite of programs.[59] The final 20 lowest

energy conformers were retained and were subjected to geometry and frequency calculations using the density functional theory (DFT) at the B3LYP/6-311+G(d,p) level. Degenerate structures were removed in the case of input structures converging into the same final geometry. For all calculations, it was ensured that every conformer had a geometry absence of an imaginary frequency, which implies that the true energy minimum had been reached. The calculations yielded the enthalpy and the Gibbs free energy (corrected to 298 K) for each conformation.

The second approach utilizes a new computational program called CREST (abbreviated from Conformer-Rotamer Ensemble Sampling Tool).[60] CREST employs a new scheme for the generation of conformational ensembles based on direct sampling at a semiempirical quantum chemical level, which makes use of multiple iterative cycles involving tight binding geometry optimization (GFNn-xTB), metadynamic (MTD) sampling, and genetic Z-matrix crossing.[61] The term GFNn-xTB stands for Geometry, frequency, and Noncovalent interactions-extended Tight-Binding, which is a computational method for structural properties develop by Grimmer and co-workers.[62] Our procedure began with building the initial peptide structure with beta-sheet dihedral angles using the Spartan'14 software. The initial structure was sent to the CREST program to generate conformational ensembles with the default energy window of 6 kcal/mol. The ensembles consisted of 150-250 conformations for the neutral tripeptides and 40-50 conformations for the charged peptides. All conformations in the ensembles were subjected to geometry optimization and frequency calculations at the B3LYP/6-311+G(d,p) level of theory to yield enthalpy and Gibbs free energy (corrected to 298 K). Degenerate structures were removed.

For each neutral and charged peptide, the unique conformations obtained from both approaches were combined and ranked in Gibbs free energies. A set of the lowest energy conformations was selected to represent an individual peptide species. The first lowest energy

conformation was located by both approaches. Most other lowest energy conformations were found from the CREST conformational search. For the resulting conformations, the Boltzmann distribution was calculated based on the free energies. The Boltzmann probability, p_i, was calculated using eq. (4), where ε_i represents the Gibbs free energy relative to the lowest energy conformation, R is the fundamental gas constant (1.987×10^{-3} kcal mol^{-1} K^{-1}), and T is the temperature (298 K). The weighted average enthalpy (H_{avg}) and free energy (G_{avg}) were calculated using eq. (5), where p_i is the Boltzmann probability, and H_i and G_i are the enthalpy and free energy of individual conformation, respectively. The values of the weighted average were then used to calculate the theoretical deprotonation enthalpy ($\Delta_{acid}H_{pep}$) and the gas-phase acidity ($\Delta_{acid}G_{pep}$), by using the isodesmic proton transfer reaction shown in eq. (6), where pepH and refH represent the peptide and the reference acid, respectively. The reference acid used for the ACA/A^{d}CA systems was ethanethiol (CH_3CH_2SH) with reported deprotonated enthalpy of 355.7 ± 2.1 kcal/mol and gas-phase acidity of 348.9. ± 2.0 kcal/mol.[63, 64]

$$p_i = \frac{\exp(-\varepsilon_i/RT)}{\sum \exp(-\varepsilon_i/RT)} \tag{4}$$

$$H_{avg} = \sum (p_i H_i)$$

$$G_{avg} = \sum (p_i G_i) \tag{5}$$

$$\text{pepH} + \text{ref}^- \longrightarrow \text{pep}^- + \text{refH} \tag{6}$$

3. Results

3.1 Relative gas-phase acidity by branching ratio bracketing

The relative gas-phase acidity between the two stereoisomeric peptides was gauged by performing the CID branching ratio bracketing experiments against the same set of references acids. The resulting branching ratios, $\ln(I_{pep}^-/I_{ref}^-)$, provide a direct comparison of the relative degree of acidity between the two peptides. The higher or more positive value of a branching ratio indicates a greater gas-phase acidity of the peptide. Seven reference acids with the deprotonation enthalpy ranging from 328.4 – 337.0 kcal/mol (1374.0 – 1410.0 kJ/mol) were chosen for this study. The reference acids along with relevant thermochemical data are listed in Table 1. These compounds are halogen or cyano group substituted small carboxylic acids. The carboxyl group is the deprotonation site for a proton-bound dimer formation with the side-chain thiol group of a peptide. The CID branching ratio for each proton-bound dimer was measured at 7 collision energies from 1.50 – 3.0 eV (E_{cm}). The resulting seven sets of branching ratio are plotted in seven graphs, and are shown in Figure 1. The data take into account the secondary fragments resulting from the loss of H_2S (34 u) and the CO_2 (44 u) from the peptide and the reference acid ions, respectively. In each set, the plots of both peptides against a single reference acid appear to be parallel. In all sets, the plots of A^dDA are higher than those of ACA. The higher branching ratio of A^dCA indicates that A^dCA is a stronger gas-phase acid than ACA. A positive, negative, or near zero value of the branching ratio indicates that the ion abundance ratio (I_{pep}^-/I_{ref}^-) would be greater than one, less than one, or near one. The positive branching ratios with using 2CPA, 2BPA, MCA, and MBA as the reference acids suggest that both peptides have an apparent gas-phase acidity greater than the reference acids. While the negative branching ratios with DCA indicate that both peptides are apparently a weaker gas-phase acid than DCA.

Lastly, the branching ratios with DFA and CYA are closer to zero, suggesting that both peptides have an acidity comparable to these two reference acids.

Table 1. Reference acids used for the acidity measurements

Reference Acid	$\Delta_{acid}H_{ref}$[a] kcal mol^{-1}	$\Delta_{acid}G_{ref}$[a] kcal mol^{-1}	$\Delta_{acid}S_{ref}$[b] kcal mol^{-1}K^{-1}
2-Chloropropionic Acid (2CPA)	337.0	330.4	22.1
2-Bromopropionic Acid (2BPA)	336.8	329.8	23.5
Chloroacetic Acid (MCA)	336.5	329.0	25.2
Bromoacetic Acid (MBA)	334.8	328.2	22.1
Difluoroacetic Acid (DFA)	331.0	323.8	24.2
Cyanoacetic Acid (CYA)	330.3	323.7	22.1
Dichloroacetic Acid (DCA)	328.4	321.9	21.8
Average (avg)[c]	333.5	326.7	23.0

[a] Values of $\Delta_{acid}H_{ref}$ and $\Delta_{acid}G_{ref}$ are taken from database in the NIST Chemistry WebBook.[63] The average uncertainty is assumed to be ±2.0 kcal mol^{-1} K^{-1}.

[b] Values of $\Delta_{acid}S_{ref}$ are calculated from $\Delta_{acid}H_{ref}$ and $\Delta_{acid}G_{ref}$ using the relationship $\Delta G = \Delta H - T(\Delta S)$, where T = 298 K. The average uncertainty is assumed to be ±2.0 cal mol^{-1} K^{-1}.

[c] Values are arithmetic average, where $\Delta_{acid}H_{avg}$ = 333.5 kcal/mol and $\Delta_{acid}S_{avg}$ = 23.0 cal/mol K.

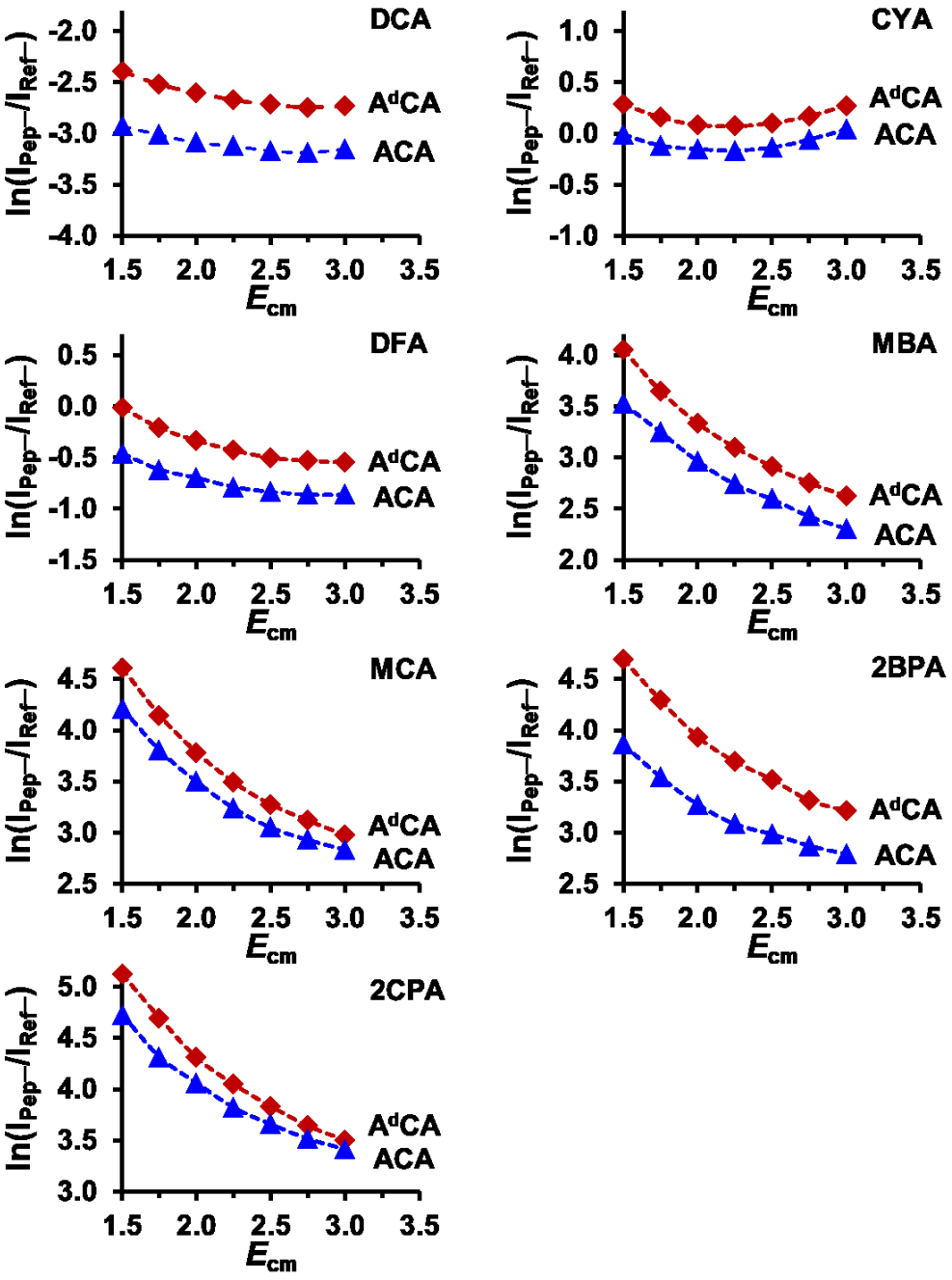

Figure 1. Plots of CID branching ratios ($ln[(I_{pep}^-)/(I_{ref}^-)]$) against collision energies (E_{cm}) for the dissociation of the proton-bound dimers of the two peptides with seven reference acids. The reference acids are shown in Abbreviations in the seven graphs. Data were collected at 7 collision energies from 1.5-3.0 eV (E_{cm}). Each graph shows the branching ratio plots for the two peptides against a single reference acid, where the plot with blue triangles is for ACA and the plot with red squares is for A^dCA.

3.2 Gas-phase acidity by the extended kinetic method

The quantitative values of the deprotonation enthalpy ($\Delta_{acid}H_{pep}$) for the two peptides were determined using the extended kinetic method (EKM). The CID product ion branching ratios of the two peptides against the seven reference acids are shown in Table 2. The collision energies used in these experiments were from 1.5 – 3.0 eV (E_{cm}). At lower collision energies, the data were scatted, and at higher collision energies, the data were skewed by secondary and tertiary fragmentations. The thermo-kinetic plots of $ln([I_{pep}^-]/[I_{ref}^-])$ against $\Delta_{acid}H_{ref} - \Delta_{acid}H_{avg}$ are shown in Figure 2a. Linear regression of the plots yielded the slope of $1/RT_{eff}$ and the y-intercept of $Y = -[(\Delta_{acid}H_{pep} - \Delta_{acid}H_{avg})/RT_{eff} - \Delta(\Delta_{acid}S)/R]$. The resulting values are presented in Table 3. These values were used to construct the thermo-kinetic plots of Y against $1/RT_{eff}$, shown in Figure 2b. Linear regression of the plots yielded the slope corresponding to the term $\Delta_{acid}H_{avg} - \Delta_{acid}H_{pep}$ and y-intercept corresponding to the term $(\Delta_{acid}S_{pep} - \Delta_{acid}S_{avg})/R$, also shown in Table 3. Using the values of $\Delta_{acid}H_{avg}$ and $\Delta_{acid}S_{avg}$ shown in Table 1, $\Delta_{acid}H_{pep}$ for ACA and A^dCA were determined to be be 328.0 ± 2.2 kcal/mol (1372.4 ± 9.2 kJ/mol) and 327.8 ± 2.2 kcal/mol (1371.5 ± 9.2 kJ/mol), and $\Delta_{acid}S_{pep}$ were determined to be 17.7 ± 2.7 and 18.1 ± 2.7 cal/mol K (74.1 ± 11.3 and 75.7 ± 11.3 J/mol K), respectively, shown in Table 4. Finally, the gas-phase acidities in the form of free-energy ($\Delta_{acid}G_{pep}$, eq. (3)), were determined to be 322.7 ± 2.2 kcal/mol (1350.2 ± 9.2 kJ/mol) and 322.4 ± 2.2 kcal/mol (1348.9 ± 9.2 kJ/mol), respectively, also shown in Table 4.

Notice that the errors assigned to the thermochemical values are the absolute uncertainties. The absolute uncertainties are mainly due to the errors associated with the gas-phase acidity scale of the reference acids. Since the same set of reference acids was used for the two peptide systems, the uncertainties in the relative gas-phase acidities between the two peptide systems are largely canceled out. Using the statistical analysis of standard deviation of the

experimental data measured in multiple days, the relative uncertainty of the thermochemical values was estimated to be ±0.1 kcal/mol (0.4 kJ/mol). An example is shown in Table S1.

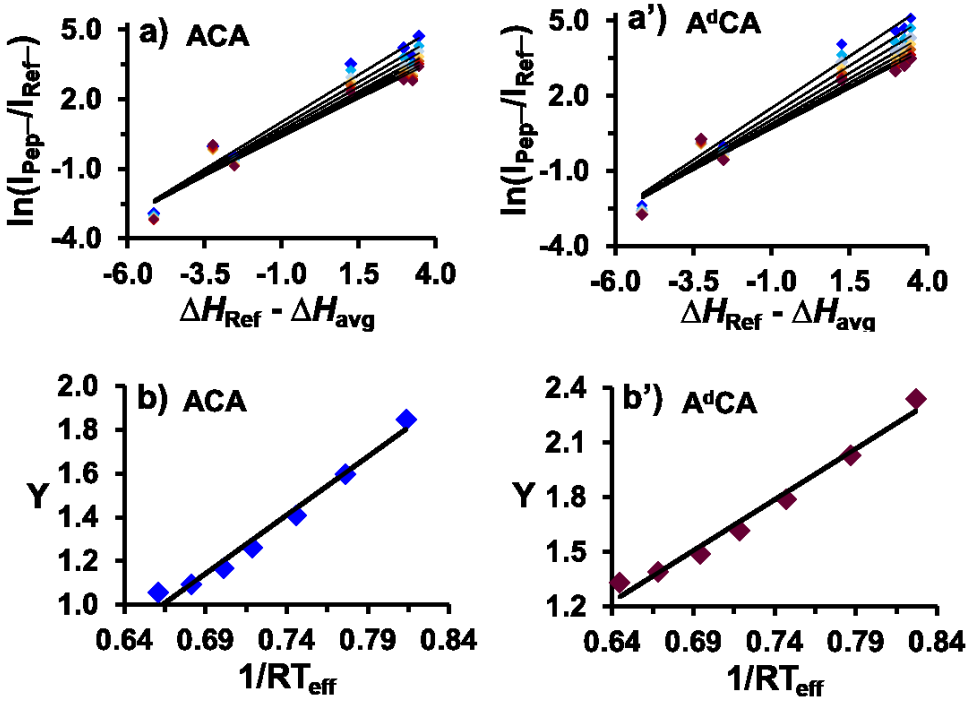

Figure 2: Thermo-kinetic plots for the two peptide systems, ACA and A^{d}CA. a) Plots of $ln([I_{pep}^{-}]/[I_{ref}^{-}])$ against $\Delta_{acid}H_{ref} - \Delta_{acid}H_{avg.}$, and b) Plots of $Y = -[(\Delta_{acid}H_{pep} - \Delta_{acid}H_{avg})/RT_{eff} - \Delta(\Delta_{acid}S)/R]$ against $1/RT_{eff}$. Data were collected at seven collision energies from 1.5 – 3.0 eV (E_{cm}).

Table 2: The CID branching ratios of ACA and A^{d}CA against seven reference acids at seven collision energies

		Collision Energy (E_{cm})						
Peptide	Reference Acid	1.50 eV	1.75 eV	2.00 eV	2.25 eV	2.50 eV	2.75 eV	3.00 eV
ACA	2CPA	4.72	4.31	4.06	3.82	3.66	3.52	3.42
	2BPA	3.87	3.55	3.28	3.09	2.99	2.87	2.79
	MCA	4.21	3.81	3.50	3.24	3.05	2.93	2.84
	MBA	3.53	3.25	2.97	2.74	2.60	2.43	2.31
	DFA	-0.46	-0.62	-0.70	-0.79	-0.83	-0.86	-0.86
	CYA	-0.01	-0.12	-0.15	-0.17	-0.14	-0.06	0.04
	DCA	-2.93	-3.01	-3.08	-3.12	-3.17	-3.18	-3.15
A^{d}CA	2CPA	5.12	4.70	4.31	4.05	3.84	3.65	3.51
	2BPA	4.69	4.30	3.94	3.69	3.52	3.32	3.22
	MCA	4.61	4.15	3.78	3.49	3.28	3.12	2.98
	MBA	4.06	3.65	3.33	3.10	2.91	2.75	2.62
	DFA	-0.01	-0.21	-0.33	-0.43	-0.50	-0.53	-0.54
	CYA	0.29	0.16	0.09	0.07	0.11	0.17	0.28
	DCA	-2.39	-2.52	-2.60	-2.67	-2.72	-2.74	-2.73

Table 3: Values resulting from linear regression of two sets of thermo-kinetic plots for the ACA and A^{d}CA systems

		Collision Energy (E_{cm})						
		1.50 eV	1.75 eV	2.00 eV	2.25 eV	2.50 eV	2.75 eV	3.00 eV
ACA	$1/RT_{eff}$[a]	0.81 ± 0.07	0.78 ± 0.07	0.72 ± 0.08	0.72 ± 0.07	0.70 ± 0.07	0.68 ± 0.08	0.66 ± 0.08
	Y[a]	1.85 ± 0.23	1.59 ± 0.23	1.22 ± 0.25	1.26 ± 0.24	1.16 ± 0.24	1.09 ± 0.25	1.05 ± 0.26
	$\Delta(\Delta_{acid}H)$[b]	5.53 ± 0.44						
	$(\Delta(\Delta_{acid}S)/R$[b]	-2.70 ± 0.32						
	$(\Delta(\Delta_{acid}S)$	-5.36 ± 0.64						
A^{d}CA	$1/RT_{eff}$[a]	0.83 ± 0.06	0.79 ± 0.06	0.72 ± 0.07	0.72 ± 0.06	0.69 ± 0.07	0.67 ± 0.07	0.65 ± 0.07
	Y[a]	2.34 ± 0.19	2.03 ± 0.19	1.56 ± 0.22	1.61 ± 0.21	1.49 ± 0.22	1.39 ± 0.23	1.33 ± 0.24
	$\Delta(\Delta_{acid}H)$[b]	5.74 ± 0.45						
	$(\Delta(\Delta_{acid}S)/R$[b]	-2.48 ± 0.33						
	$(\Delta(\Delta_{acid}S)$	-4.92 ± 0.65						

[a] Results from the first set of the thermo-kinetic plots. The slope is represented by $1/RT_{eff}$, and the y-intercept is represented by $Y = -[(\Delta_{acid}H_{pep} - \Delta_{acid}H_{avg})/RT_{eff} - (\Delta(\Delta_{acid}S)/R]$.

[b] Results from the second set of the thermo-kinetic plots. The slope is represented by $\Delta(\Delta_{acid}H) = \Delta_{acid}H_{avg} - \Delta_{acid}H_{pep}$, and the y-intercept is represented by $(\Delta(\Delta_{acid}S)/R = (\Delta_{acid}S_{pep} - \Delta_{acid}S_{avg})/R$.

Table 4: Summary of the thermochemical values obtained from experimental and computation for ACA and A^{d}CA

Peptide	$\Delta_{acid}H_{pep}$[a] kcal/mol (kJ/mol)[d]	$\Delta_{acid}G_{pep}$[b] kcal/mol (kJ/mol)[d]	$\Delta_{acid}S_{pep}$[a] cal/mol K (J/mol K)[d]	$\Delta_{acid}H_{calc}$[c] kcal/mol (kJ/mol)[d]	$\Delta_{acid}G_{calc}$[c] kcal/mol (kJ/mol)[d]
ACA[e]	328.0 ± 2.2	322.7 ± 2.2	17.7 ± 2.7	327.2	321.3
	(1372.4 ± 9.2)[d]	(1350.2 ± 9.2)[d]	(74.1 ± 11.3)[d]	(1369.0)[d]	(1344.3)[d]
A^{d}CA[e]	327.8 ± 2.2	322.4 ± 2.2	18.1 ± 2.7	326.7	319.8
	(1371.5 ± 9.2)[d]	(1348.9 ± 9.2)[d]	(75.7 ± 11.3)[d]	(1366.9)[d]	(1338.0)[d]

[a] Values determined using the extended kinetic method.
[b] Values obtained using eq. (3) where T = 298 K.
[c] Values obtained using eq. (6) based on the Boltzmann averaged enthalpies and free energies of the lowest energy conformations, where the energetics of the conformations were calculated at the B3LYP/6-311+G(d,p) level of theory.
[d] Values in parenthesis are in kJ/mol or J/mol K, respectively.
[e]The relative uncertainty in the thermochemical values was estimated to be ±0.1 kcal/mol (±0.4 kJ/mol).

3.3 Computational results

A conformational search was carried out via two ways, the step-wise funneling approach (using the MMFF force field for initial conformational search) and the CREST computational procedure. The conformations generated by both methods were subjected to geometry and frequency calculations using the density functional theory (DFT) at the B3LYP/6-311+G(d,p) level. The resulting conformations were combined and degenerate ones were removed. For each peptide species, the 10 lowest energy conformations with unique geometric features were selected as the final set of conformations. The free energies associated with the conformations were used to rank them on the energy ladder. The results are summarized in Table 5, Table S2, and Figure S1. The symbols N1-N10 and N1'-N10' indicate the conformations of the neutral

peptides ACA and A^dCA, respectively, with 1 and 1' having the lowest free energy. Similarly, the symbols A1-A10 and A1'-A10' indicate the conformations of the deprotonated peptides $[ACA-H]^-$ and $[A^dCA-H]^-$, respectively. The conformations located via one or both approaches are indicated in Table S2. The two lowest-energy conformations for each peptide species are shown in Figure 3, where the dashed lines indicate hydrogen-bonding interactions between the negatively charged sulfur atom and the nearby N-H groups, and the values indicate the distance between the sulfur and the hydrogen atoms. Apparently, both neutral peptides adopt "coiled" conformations, while the shape for A^dCA appears to be more compact. The lowest energy conformations of $[ACA-H]^-$ appear to be "linear" with two hydrogen-bonding interactions, and of $[A^dCA-H]^-$ appear to be "bent" with three hydrogen-bonding interactions.

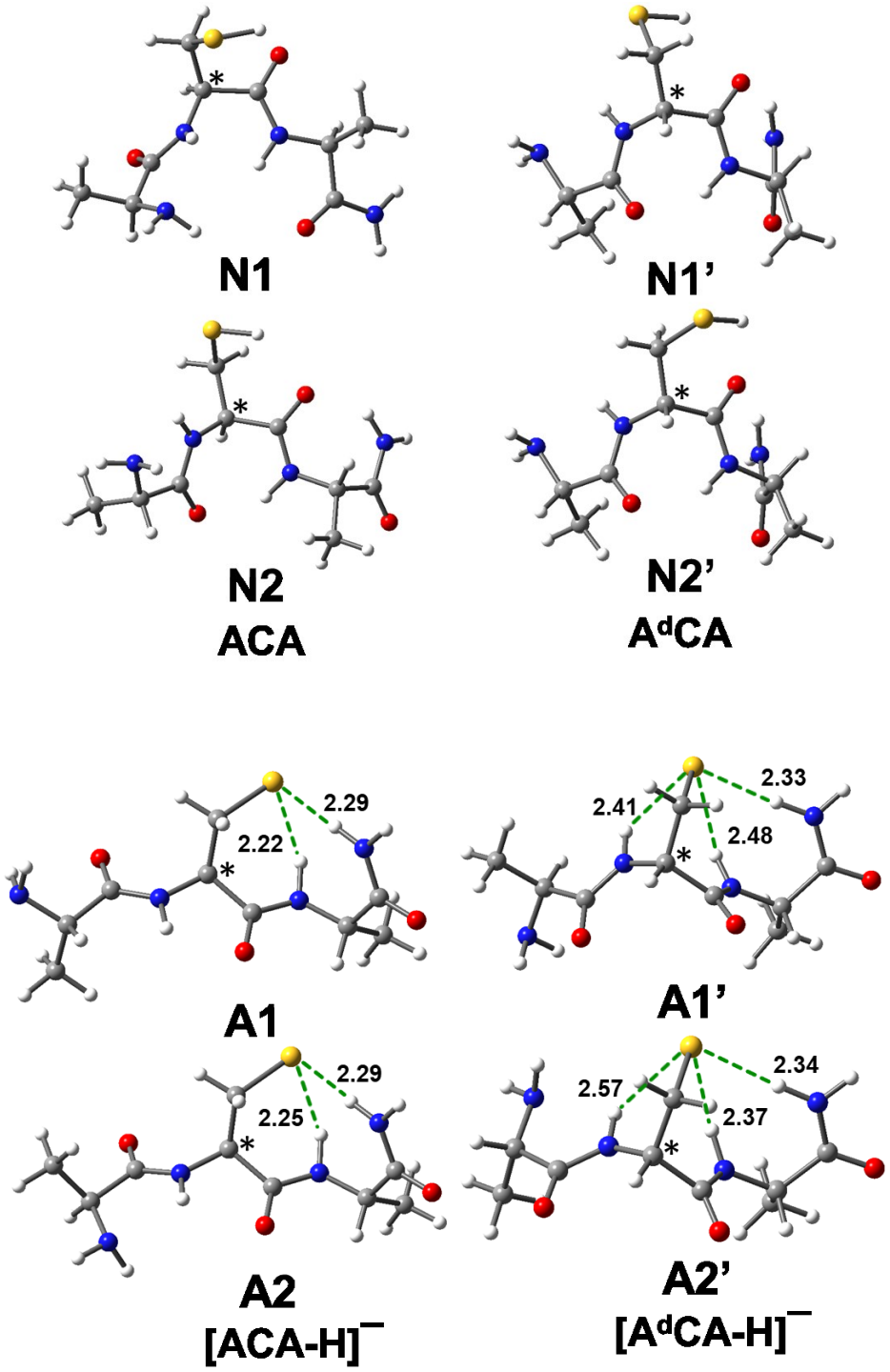

Figure 3: The two lowest energy conformations of the neutral and deprotonated peptides, where N1 and N2 for ACA, N1' and N2' for A^dCA, A1 and A2 for $[ACA-H]^-$, and A1' and A2' for $[A^dCA-H]^-$. The chiral center of the Cys residue is indicated with "*". The dashed lines indicate hydrogen-bonding interactions and the values (Å) indicate the distance between the sulfur and the hydrogen atoms involved in the hydrogen bonds.

The calculated energetic values for all 10 conformations of each peptide species are listed in Table S2, which includes the enthalpy/free energy, relative enthalpy/free energy, weighted average of enthalpy/free energy, and the Boltzmann probability. A summary of the relative energetic values and Boltzmann probability is shown in Table. 5, where the conformations are ranked in free energy. For each peptide species, the first conformation is assigned as the reference with 0.0 kcal/mol in free energy. The relative free energies of other conformations are calculated accordingly. The relative enthalpies associated with the set of conformations are listed according to the rank for their free energies. The Boltzmann probabilities for each set of conformations are calculated based on free energies using eq. (4). The energetic data show that both neutral peptides have the 10 conformations within 1.5 kcal/mol in free energy. The lowest energy conformation contributes about 30% to the population. The second and third conformations contribute 30-35%. While for the deprotonated peptides, the 10 conformations span a wider energy range of about 3.0-5.0 kcal/mol. The lowest energy conformation contributes 78% to $[ACA\text{-}H]^-$ and 97% to $[A^dCA\text{-}H]^-$.

The weighted average of enthalpy (H_{avg}) and free energy (G_{avg}) associated with the 10 conformations were calculated using eq. (5). The results are shown at the bottom of each set of the conformations in Table 5. In order to compare the relative stability between the L-cysteine and the D-cysteine peptides, the relative enthalpy (Rel. H_{avg}) and free energy (Rel. G_{avg}) were calculated using the weighted average of enthalpy and free energy, respectively. As shown in Table 5, the two neutral peptides, ACA and AdCA, have about the same enthalpy and free energy (within 0.4 kcal/mol). While $[A^dCA\text{-}H]^-$ has a lower enthalpy (by 1.0 kcal/mol) and a lower free energy (by 1.5 kcal/mol) than $[ACA\text{-}H]^-$, suggesting that $[A^dCA\text{-}H]^-$ is more stable.

The weighted average of enthalpy and free energy were used to calculate the deprotonation enthalpy and the gas-phase acidity of the peptides. Ethanethiol (CH_3CH_2SH, $\Delta_{acid}H$ = 355.7 kcal/mol, $\Delta_{acid}G$ = 348.9 kcal/mol)[63] was used as the reference acid. The calculated enthalpy and free energy of the neutral and deprotonated enthanethiol are shown in Table S2. By using eq. (6), the values of the deprotonation enthalpy ($\Delta_{acid}H_{calc}$) and the gas-phase acidity ($\Delta_{acid}G_{calc}$) were calculated to be 327.2 and 321.3 kcal/mol (1369.0 and 1344.3 kJ/mol) for ACA, and 326.7 and 319.8 kcal/mol (1366.9 and 1338.0 kJ/mol) for A^dCA, respectively. The values are in good agreement with the results from the experiments, shown in Table 4.

Table 5: Summary of calculated energetics and Boltzmann distributions of the conformations obtained for ACA and A^{d}CA

Conf.	ΔH^{a}	ΔG^{a}	P_i (%)[b]	Conf.	ΔH^{a}	ΔG^{a}	P_i (%)[b]
ACA				$[ACA-H]^-$			
N1	0.0	0.0	30.0%	A1	0.0	0.0	78.2%
N2	-1.9	0.1	25.1%	A2	1.7	1.3	9.5%
N3	-0.4	0.6	10.5%	A3	1.8	1.8	3.6%
N4	-0.6	0.8	8.0%	A4	2.9	2.1	2.2%
N5	-0.1	0.9	6.1%	A5	2.6	2.2	1.9%
N6	0.1	1.1	5.0%	A6	3.0	2.3	1.7%
N7	-0.1	1.1	4.7%	A7	3.9	2.3	1.6%
8N	1.9	1.2	3.9%	A8	4.1	2.9	0.6%
N9	1.2	1.2	3.9%	A9	2.7	3.1	0.5%
N10	1.8	1.4	2.8%	A10	4.8	3.2	0.4%
H_{avg}[c]	-1196.6968			H_{avg}[c]	-1196.1807		
G_{avg}[c]	-1196.7685			G_{avg}[c]	-1196.2498		
Rel. H_{avg}[d]	0.0			*Rel.* H_{avg}[d]	0.0		
Rel. G_{avg}[d]	0.0			*Rel.* G_{avg}[d]	0.0		
A^{d}CA				$[A^{d}CA-H]^-$			
N1’	0.0	0.0	31.9%	A1’	0.0	0.0	97.5%
N2’	0.5	0.2	21.4%	A2’	2.8	2.5	1.4%
N3’	1.6	0.7	10.6%	A3’	2.6	3.0	0.6%
N4’	2.1	0.8	8.0%	A4’	4.0	3.8	0.2%
N5’	3.0	0.9	7.3%	A5’	4.1	3.9	0.1%
N6’	2.1	0.9	6.5%	A6’	3.4	4.2	0.1%
N7’	1.6	1.2	4.4%	A7’	4.7	4.3	0.1%
N8’	2.3	1.2	3.9%	A8’	4.6	4.6	0.0%
N9’	1.7	1.3	3.4%	A9’	5.2	5.1	0.0%
N10’	2.0	1.5	2.6%	A10’	5.4	5.3	0.0%
H_{avg}[c]	-1196.6975			H_{avg}[c]	-1196.1823		
G_{avg}[c]	-1196.7684			G_{avg}[c]	-1196.2522		
Rel. H_{avg}[d]	-0.4			*Rel.* H_{avg}[d]	-1.0		
Rel. G_{avg}[d]	0.1			*Rel.* G_{avg}[d]	-1.5		

[a] Values (kcal/mol) obtained from calculations at the B3LYP/6-311+G(d,p) level of theory.
[b] Boltzmann probability calculated using eq. (4).
[c] Weighted average of enthalpy and free energy (Hartree) of the 10 conformations calculated using eq. (5), where the values of enthalpy and free energy for all conformations are shown in Table S2.
[d] Relative enthalpy and free energy (kcal/mol) between ACA and AdCA, and between $[ACA-H]^-$ and $[A^{d}CA-H]^-$, calculated using the weighted average of H_{avg} and G_{avg}, respectively.

4. Discussion

The CID branching ratio bracketing results shown in Figure 1 suggest that A^dCA is a stronger gas-phase acid than ACA. Quantitatively, A^dCA is more acidic than ACA by about 0.3 kcal/mol (1.3 kJ/mol) determined by using the extended kinetic method. As shown in Table 4, the gas-phase deprotonation enthalpies of ACA and A^dCA are measured to be 328.0 ± 2.2 kcal/mol (1372.4 ± 9.2 kJ/mol) and 327.8 ± 2.2 kcal/mol (1371.5 ± 9.2 kJ/mol), respectively, and the corresponding gas-phase acidities are 322.7 ± 2.2 kcal/mol (1350.2 ± 9.2 kJ/mol) and 322.4 ± 2.2 kcal/mol (1348.9 ± 9.2 kJ/mol), respectively. The theoretical predictions agree with the experiments. Also shown in Table 4, the calculated deprotonation enthalpy and free energy of A^dCA are 0.5 kcal/mol (2.1 kJ/mol) and 1.5 kcal/mol (6.3 kJ/mol) lower than those of ACA, suggesting A^dCA to be a stronger gas-phase acid. Although the quantitative difference is small, both experiments and calculations clearly show that converting the cysteine residue from the L-form to the D-form enhances the gas-phase acidity.

Since the gas-phase acidity is associated with both the neutral and the charged form of a peptide, changing in the energy (stability) of either form could cause the perturbation in the acidity. As indicated by the values of relative free energy (*Rel.* G_{avg}) shown in Table 5, ACA and A^dCA have a comparable energy or stability, while $[A^dCA\text{-}H]^-$ is lower in energy than $[ACA\text{-}H]^-$ by 1.5 kcal/mol, suggesting that the energy difference in the deprotonated peptides is the main contribution to the difference in the gas-phase acidity. In other words, the higher stability of $[A^dCA\text{-}H]^-$ is the main source of the grater gas-phase acidity of A^dCA. The same conclusion can be obtained by comparing the values of the relative enthalpy (*Rel.* H_{avg}). Our previous studies about isomeric di-and tripeptides also show that the difference in the gas-phase acidities

or proton affinities is mainly come from the relative stabilities of the charged molecules in the form of deprotonated or protonated peptides, respectively.[28, 30]

The relative stability of the peptides is reflected in the structural features. As shown in Figure 3, the neutral peptides are all adopted "coiled" or "folded" conformations, although the shape of A^{d}CA appears to be more compact. This may explain the similarity in enthalpy and free energy of the two peptides. The conformational features of the deprotonated peptides are quite different from those of the neutral ones. The lowest energy conformations of $[ACA\text{-}H]^-$ appear to be "extended" or "linear" with two main S---H-N hydrogen bonds. The lowest energy conformations of $[A^{d}CA\text{-}H]^-$ appear to be "bent" with three main S---H-N hydrogen bonds. The bent conformation allows for more hydrogen-bonding interactions between the negatively charged sulfur atom and the N-H groups, which ultimately stabilizes the charged peptide. Stabilization of deprotonated peptides due to adopting a more compact conformation was also observed in di- and tripeptides in our previous studies.[28]

The results from this study suggest that changing the chirality at the cysteine residue alters the conformation as well as the stability of the peptide ions upon deprotonation. While the alteration is subtle in the small model peptides, the chirality effect could be magnified in longer peptides or in biological systems where the cysteine residue is a part of the active site motif. One example is a recent study of incorporating a D-cysteine into a metalloprotein, which results in enhanced binding to metal ions.[37] In this case, the side-chain of the D-cysteine is pre-organized into a suitable geometry which allows a more efficient binding to a metal ion. Although the results from the current study do not directly explain the enhanced biological activity of D-AA containing peptides, such as those isolated from molluscs,[13] the findings show that incorporating

a single D-AA into a peptide could modify the chemistry as well as the biochemistry of the peptide.

5. Conclusions

The gas-phase acidities and conformations of two stereoisomeric tripeptides containing a D/L-cysteine, ACA and A^{d}CA, have been studied experimentally and computationally. The CID branching ratio bracketing experiments clearly show that A^{d}CA is a stronger gas-phase acid than ACA. Using the extended kinetic method, the gas-phase deprotonation enthalpies ($\Delta_{acid}H$) of the ACA and A^{d}CA have been determined to be 328.0 ± 2.2 kcal/mol (1372.4 ± 9.2 kJ/mol) and 327.8 ± 2.2 kcal/mol (1371.5 ± 9.2 kJ/mol), respectively. The corresponding gas-phase acidities ($\Delta_{acid}G$) have been determined to be 322.7 ± 2.2 kcal/mol (1350.2 ± 9.2 kJ/mol) and 322.4 ± 2.2 kcal/mol (1348.9 ± 9.2 kJ/mol), respectively, with the difference of 0.3 kcal/mol (1.3 kJ/mol) in favor of A^{d}CA. Computational studies indicate that the stronger acidity in A^{d}CA is mainly due to the higher stability of the peptide ion, [A^{d}CA-H]$^{-}$. The lowest energy conformations of [A^{d}CA-H]$^{-}$ appears to be "bent", while of [ACA-H]$^{-}$ appear to be "linear". The bent conformation allows more efficient hydrogen-bonding interactions between the negatively charged thiolate group (S^{-}) and the vicinal N-H groups within [A^{d}CA-H]$^{-}$, which stabilizes the ion. The study shows that the chirality change at a single amino acid residue can alter the intrinsic chemistry of oligopeptides. The chirality effect could be magnified in longer peptides and in proteins, especially if the unique amino acid is located at the active sites.

Supporting Information Description

Sample analysis of standard deviation of the experimental gas-phase acidity values is given in Table S1. Summaries of the calculated energetic values for the ACA and A^{d}CA systems are given in Tables S2a and S2b. Four sets of the 10 lowest energy conformations in the ZYZ format corresponding to neutral and deprotonated peptides are given in Figures S1(a-d).

Acknowledgements

This work was supported in part by a grant from the National Science Foundation (CHE-1954833). Y. Zhang, Z. Buen, M. Browne, Y. Mann thank the graduate research support from the University of the Pacific. All mass spectrometry experiments were conducted at the Chemistry Mass Spectrometry Facility at the University of the Pacific.

References

1. Genchi, G., An overview on D-amino acids. *Amino Acids* **2017,** *49*, 1521-1533.
2. Sasabe, J.; Suzuki, M.; Suzuki, M., Distinctive Roles of D-Amino Acids in the Homochiral World: Chirality of Amino Acids Modulates Mammalian Physiology and Pathology. *Keio J Med* **2018**.
3. Ollivaux, C.; Soyez, D.; Toullec, J.-Y., Biogenesis of D-amino acid containing peptides/proteins: where, when and how? *J. Pept. Sci.* **2014,** *20*, 595-612.
4. Cava, F.; Lam, H.; de, P., Miguel A.; Waldor, M. K., Emerging knowledge of regulatory roles of D-amino acids in bacteria. *Cell. Mol. Life Sci.* **2011,** *68*, 817-831.
5. Fuchs, S. A.; Berger, R.; Klomp, L. W. J.; de Koning, T. J., d-Amino acids in the central nervous system in health and disease. *Molecular Genetics and Metabolism* **2005,** *85*, 168-180.
6. Kiriyama, Y.; Nochi, H., D-Amino Acids in the Nervous and Endocrine Systems. *Scientifica (Cairo)* **2016,** *2016*, 6494621.
7. Tomiyama, T.; Asano, S.; Furiya, Y.; Shirasawa, T.; Endo, N.; Mori, H., Racemization of Asp23 residue affects the aggregation properties of Alzheimer amyloid β protein analogs. *J. Biol. Chem.* **1994,** *269*, 10205-8.
8. Roher, A. E.; Lowenson, J. D.; Clarke, S.; Wolkow, C.; Wang, R.; Cotter, R. J.; Reardon, I. M.; Zurcher-Neely, H. A.; Heinrikson, R. L.; Ball, M. J.; Greenberg, B. D., Structural alterations in the peptide backbone of Î²-amyloid core protein may account for its deposition and stability in Alzheimer's disease. *J. Biol. Chem.* **1993,** *268*, 3072-83.
9. Kaji, Y.; Oshika, T.; Takazawa, Y.; Fukayama, M.; Fujii, N. In *Accumulation of D-β-aspartic acid-containing proteins in age-related ocular diseases*2011 Verlag Helvetica Chimica Acta; pp 31-37.
10. Fujii, N.; Kaji, Y.; Fujii, N.; Nakamura, T.; Motoie, R.; Mori, Y.; Kinouchi, T., Collapse of Homochirality of Amino Acids in Proteins from Various Tissues during Aging. *Chem. Biodiversity* **2010,** *7*, 1389-1397.
11. Selkoe, D. J., Folding proteins in fatal ways. *Nature* **2003,** *426*, 900-904.
12. Montecucchi, P. C.; De Castiglione, R.; Piani, S.; Gozzini, L.; Erspamer, V., Amino acid composition and sequence of dermorphin, a novel opiate-like peptide from the skin of Phyllomedusa sauvagei. *Int. J. Pept. Protein Res.* **1981,** *17*, 275-83.
13. Bai, L.; Sheeley, S.; Sweedler, J. V., Analysis of Endogenous D-Amino Acid-Containing Peptides in Metazoa. *Bioanal Rev* **2009,** *1*, 7-24.
14. Jilek, A.; Kreil, G., D-Amino Acids in Animal Peptides. *Monatsh. Chem.* **2008,** *139*, 1-5.
15. Bai, L.; Romanova, E. V.; Sweedler, J. V., Distinguishing endogenous D-amino acid-containing neuropeptides in individual neurons using tandem mass spectrometry. *Anal. Chem. (Washington, DC, U. S.)* **2011,** *83*, 2794-2800.
16. Adams, C. M.; Zubarev, R. A., Distinguishing and Quantifying Peptides and Proteins Containing D-Amino Acids by Tandem Mass Spectrometry. *Anal. Chem.* **2005,** *77*, 4571-4580.
17. Wu, L.; Cooks, R. G., Chiral Analysis Using the Kinetic Method with Optimized Fixed Ligands: Applications to Some Antibiotics. *Anal. Chem.* **2003,** *75*, 678-684.
18. Serafin, S. V.; Maranan, R.; Zhang, K.; Morton, T. H., Mass Spectrometric Differentiation of Linear Peptides Composed of L-Amino Acids from Isomers Containing One D-Amino Acid Residue. *Anal. Chem.* **2005,** *77*, 5480-5487.
19. Jeanne Dit Fouque, K.; Garabedian, A.; Porter, J.; Baird, M.; Pang, X.; Williams, T. D.; Li, L.; Shvartsburg, A.; Fernandez-Lima, F., Fast and Effective Ion Mobility-Mass Spectrometry

Separation of D-Amino-Acid-Containing Peptides. *Anal. Chem. (Washington, DC, U. S.)* **2017,** *89*, 11787-11794.
20. Pang, X.; Jia, C.; Chen, Z.; Li, L., Structural Characterization of Monomers and Oligomers of D-Amino Acid-Containing Peptides Using T-Wave Ion Mobility Mass Spectrometry. *J. Am. Soc. Mass Spectrom.* **2017,** *28*, 110-118.
21. Jia, C.; Lietz, C. B.; Yu, Q.; Li, L., Site-Specific Characterization of d-Amino Acid Containing Peptide Epimers by Ion Mobility Spectrometry. *Anal. Chem. (Washington, DC, U. S.)* **2014,** *86*, 2972-2981.
22. Demarchi, B.; Collins, M.; Bergstrom, E.; Dowle, A.; Penkman, K.; Thomas-Oates, J.; Wilson, J., New Experimental Evidence for In-Chain Amino Acid Racemization of Serine in a Model Peptide. *Anal. Chem. (Washington, DC, U. S.)* **2013,** *85*, 5835-5842.
23. Livnat, I.; Tai, H.-C.; Jansson, E. T.; Bai, L.; Romanova, E. V.; Chen, T.-t.; Yu, K.; Chen, S.-a.; Zhang, Y.; Wang, Z.-y.; Liu, D.-d.; Weiss, K. R.; Jing, J.; Sweedler, J. V., A D-Amino Acid-Containing Neuropeptide Discovery Funnel. *Anal. Chem. (Washington, DC, U. S.)* **2016,** *88*, 11868-11876.
24. Cui, C.; McNeill, A. S.; Jackson, W. C.; Raddatz, M. A.; Stover, M. L.; Dixon, D. A.; Cassady, C. J., Experimental and Computational Study of the Gas-Phase Acidities of Acidic Di- and Tripeptides. *J. Phys. Chem. B* **2019,** *123*, 606-613.
25. Vaisar, T.; Urban, J.; Nakanishi, H., Peptide diastereoisomers show different proton affinities. *J. Mass Spectrom.* **1996,** *31*, 937-939.
26. Ren, J.; Tan, J. P.; Harper, R. T., Gas-Phase Acidities of Cysteine-Polyalanine Peptides I: A3,4CSH and HSCA3,4. *J. Phys. Chem. A* **2009,** *113*, 10903-10912.
27. Morishetti, K. K.; Huang, B. D. S.; Yates, J. M.; Ren, J., Gas-Phase Acidities of Cysteine-Polyglycine Peptides: The Effect of the Cysteine Position. *J. Am. Soc. Mass Spectrom.* **2010,** *21*, 603-614.
28. Shen, J.; Ren, J., Gas phase acidity of a cysteine residue in small oligopeptides. *Int. J. Mass Spectrom.* **2012,** *316-318*, 147-156.
29. Batoon, P.; Ren, J., Proton affinity of dipeptides containing alanine and diaminobutyric acid. *Int. J. Mass Spectrom.* **2015,** *378*, 151-159.
30. Batoon, P.; Ren, J., Proton affinity of isomeric dipeptides containing lysine and non-proteinogenic lysine homologues. *J. Phys. Chem. B* **2016,** *120*, 7783-7794.
31. Martin, J. L., Thioredoxin-a fold for all reasons. *Structure* **1995,** *3*, 245-250.
32. Takahashi, N.; Creighton, T. E., On the Reactivity and Ionization of the Active Site Cysteine Residues of Escherichia coli Thioredoxin. *Biochemistry* **1996,** *35*, 8342-8353.
33. Gan, Z. R.; Sardana, M. K.; Jacobs, J. W.; Polokoff, M. A., Yeast thioltransferase - the active site cysteines display differential reactivity. *Archives of Biochemistry and Biophysics* **1990,** *282*, 110-115.
34. Kortemme, T.; Darby, N. J.; Creighton, T. E., Electrostatic interactions in the active site of the N-terminal thioredoxin-like domain of protein disulfide isomerase. *Biochemistry* **1996,** *35*, 14503-14511.
35. Philipps, B.; Glockshuber, R., Randomization of the Entire Active-site Helix alpha 1 of the Thiol-disulfide Oxidoreductase DsbA from Escherichia coli. *J. Biol. Chem.* **2002,** *277*, 43050-43057.
36. Jocelyn, P. C., *Biochemistry of the SH Group. The Occurrence, Chemical Properties, Metabolism, and Biological Function of Thiols and Disulfides*. Academic1972; p 406 pp.

37. Ruckthong, L.; Peacock, A. F. A.; Pascoe, C. E.; Hemmingsen, L.; Stuckey, J. A.; Pecoraro, V. L., D-Cysteine ligands control metal geometries within de novo designed three-stranded coiled coils. *Chem. - Eur. J.* **2017,** *23*, 8232-8243.
38. Chan, W. C.; White, P. D.; Editors, *Fmoc Solid Phase Peptide Synthesis: A Practical Approach*. Oxford Univ Press2000; p 346 pp.
39. Amblard, M.; Fehrentz, J.-A.; Martinez, J.; Subra, G., Methods and protocols of modern solid phase peptide synthesis. *Mol. Biotechnol.* **2006,** *33*, 239-254.
40. Cooks, R. G.; Koskinen, J. T.; Thomas, P. D., The kinetic method of making thermochemical determinations. *J. Mass Spectrom.* **1999,** *34*, 85-92.
41. Cooks, R. G.; Patrick, J. S.; Kotiaho, T.; McLuckey, S. A., Thermochemical determinations by the kinetic method. *Mass Spectrom. Rev.* **1994,** *13*, 287-339.
42. Cooks, R. G.; Wong, P. S. H., Kinetic method of making thermochemical determinations: advances and applications. *Acc. Chem. Res.* **1998,** *31*, 379-386.
43. Cerda, B. A.; Wesdemiotis, C., Li+, Na+, and K+ Binding to the DNA and RNA nucleobases. Bond energies and attachment sites from the dissociation of metal ion-bound heterodimers. *J. Am. Chem. Soc.* **1996,** *118*, 11884-11892.
44. Cheng, X.; Wu, Z.; Fenselau, C., Collision energy dependence of proton-bound dimer dissociation: entropy effects, proton affinities, and intramolecular hydrogen-bonding in protonated peptides. *J. Am. Chem. Soc.* **1993,** *115*, 4844-4848.
45. Armentrout, P. B., Entropy Measurements and the Kinetic Method: a Statistically Meaningful Approach. *J. Am. Soc. Mass Spectrom.* **2000,** *11*, 371-379.
46. Ervin, K. M.; Armentrout, P. B., Systematic and random errors in ion affinities and activation entropies from the extended kinetic method. *J. Mass Spectrom.* **2004,** *39*, 1004-1015.
47. Wesdemiotis, C., Entropy considerations in kinetic method experiments. *J. Mass Spectrom.* **2004,** *39*, 998-1003.
48. Ervin, K. M., Microcanonical analysis of the kinetic method. The meaning of the "apparent entropy". *J. Am. Soc. Mass Spectrom.* **2002,** *13*, 435-452.
49. Drahos, L.; Peltz, C.; Vekey, K., Accuracy of enthalpy and entropy determination using the kinetic method: Are we approaching a consensus? *J. Mass Spectrom.* **2004,** *39*, 1016-1024.
50. Laskin, J.; Futrell, J. H., The theoretical basis of the kinetic method from the point of view of finite heat bath theory. *J. Phys. Chem. A* **2000,** *104*, 8829-8837.
51. Norrman, K.; McMahon, T. B., Relationship between effective temperature of thermalized ions and ion source temperature. *Int. J. Mass Spectrom.* **1998,** *176*, 87-97.
52. Meot-Ner, M.; Somogyi, A., A thermal extrapolation method for the effective temperatures and internal energies of activated ions. *Int. J. Mass Spectrom.* **2007,** *267*, 346-356.
53. Boggs, P. T.; Byrd, R. H.; Rogers, J. E.; Schnabel, R. B., ODRPACK Version 2.01 Software for Weighted Orthogonal Distance Regression. *Report NISTIR 92-4834. National Institute of Standards and Technology: Gaithersburg, MD* **1992**.
54. Bouchoux, G., Gas-phase basicities of polyfunctional molecules. Part 1: theory and methods. *Mass Spectrom. Rev.* **2007,** *26*, 775-835.
55. Cao, J.; Aubry, C.; Holmes, J. L., Proton affinities of simple amines; Entropies and enthalpies of activation and their effect on the kinetic method for evaluating proton affinities. *J. Phys. Chem. A* **2000,** *104*, 10045-10052.
56. Bouchoux, G.; Sablier, M.; Berruyer-Penaud, F., Obtaining thermochemical data by the extended kinetic method. *J. Mass Spectrom.* **2004,** *39*, 986-997.

57. Batoon, P.; Oomens, J.; Berden, G.; Ren, J., Conformations of Protonated AlaDap and DapAla Characterized by IRMPD Spectroscopy and Molecular Modeling. *J. Phys. Chem. B* **2018,** *122*, 2191-2202.
58. Shao, Y.; Molnar, L. F.; Jung, Y.; Kussmann, J.; Ochsenfeld, C.; Brown, S. T.; Gilbert, A. T. B.; Slipchenko, L. V.; Levchenko, S. V.; O'Neill, D. P.; DiStasio Jr, R. A.; Lochan, R. C.; Wang, T.; Beran, G. J. O.; Besley, N. A.; Herbert, J. M.; Yeh Lin, C.; Van Voorhis, T.; Hung Chien, S.; Sodt, A.; Steele, R. P.; Rassolov, V. A.; Maslen, P. E.; Korambath, P. P.; Adamson, R. D.; Austin, B.; Baker, J.; Byrd, E. F. C.; Dachsel, H.; Doerksen, R. J.; Dreuw, A.; Dunietz, B. D.; Dutoi, A. D.; Furlani, T. R.; Gwaltney, S. R.; Heyden, A.; Hirata, S.; Hsu, C.-P.; Kedziora, G.; Khalliulin, R. Z.; Klunzinger, P.; Lee, A. M.; Lee, M. S.; Liang, W.; Lotan, I.; Nair, N.; Peters, B.; Proynov, E. I.; Pieniazek, P. A.; Min Rhee, Y.; Ritchie, J.; Rosta, E.; David Sherrill, C.; Simmonett, A. C.; Subotnik, J. E.; Lee Woodcock Iii, H.; Zhang, W.; Bell, A. T.; Chakraborty, A. K.; Chipman, D. M.; Keil, F. J.; Warshel, A.; Hehre, W. J.; Schaefer Iii, H. F.; Kong, J.; Krylov, A. I.; Gill, P. M. W.; Head-Gordon, M., Advances in methods and algorithms in a modern quantum chemistry program package. *Physical Chemistry Chemical Physics* **2006,** *8*, 3172-3191.
59. Frisch, M. J.; Trucks, G. W.; Schlegel, H. B.; Scuseria, G. E.; Robb, M. A.; Cheeseman, J. R.; Scalmani, G.; Barone, V.; Petersson, G. A.; Nakatsuji, H.; Li, X.; Caricato, M.; Marenich, A. V.; Bloino, J.; Janesko, B. G.; Gomperts, R.; Mennucci, B.; Hratchian, H. P.; Ortiz, J. V.; Izmaylov, A. F.; Sonnenberg, J. L.; Williams; Ding, F.; Lipparini, F.; Egidi, F.; Goings, J.; Peng, B.; Petrone, A.; Henderson, T.; Ranasinghe, D.; Zakrzewski, V. G.; Gao, J.; Rega, N.; Zheng, G.; Liang, W.; Hada, M.; Ehara, M.; Toyota, K.; Fukuda, R.; Hasegawa, J.; Ishida, M.; Nakajima, T.; Honda, Y.; Kitao, O.; Nakai, H.; Vreven, T.; Throssell, K.; Montgomery Jr., J. A.; Peralta, J. E.; Ogliaro, F.; Bearpark, M. J.; Heyd, J. J.; Brothers, E. N.; Kudin, K. N.; Staroverov, V. N.; Keith, T. A.; Kobayashi, R.; Normand, J.; Raghavachari, K.; Rendell, A. P.; Burant, J. C.; Iyengar, S. S.; Tomasi, J.; Cossi, M.; Millam, J. M.; Klene, M.; Adamo, C.; Cammi, R.; Ochterski, J. W.; Martin, R. L.; Morokuma, K.; Farkas, O.; Foresman, J. B.; Fox, D. J. *Gaussian 16 Rev. C.01*: Wallingford, CT, 2016.
60. CREST, *https://xtb-docs.readthedocs.io/en/latest/crest.html, and https://github.com/grimme-lab/xtb/releases, opyright 2019, Grimme group Revision 3b3faf69*.
61. Pracht, P.; Bohle, F.; Grimme, S., Automated exploration of the low-energy chemical space with fast quantum chemical methods. *Phys. Chem. Chem. Phys.* **2020,** *22*, 7169-7192.
62. Grimme, S.; Bannwarth, C.; Shushkov, P., A Robust and Accurate Tight-Binding Quantum Chemical Method for Structures, Vibrational Frequencies, and Noncovalent Interactions of Large Molecular Systems Parametrized for All spd-Block Elements (Z = 1-86). *J. Chem. Theory Comput.* **2017,** *13*, 1989-2009.
63. NIST, NIST Chemistry WebBook, NIST Standard Reference Database Number 69, https://webbook.nist.gov/chemistry/. National Institute of Standards and Technology, Gaithersburg MD, 208992018.
64. Janousek, B. K.; Reed, K. J.; Brauman, J. I., Electron photodetachment from mercaptyl anions (RS-). Electron affinities of mercaptyl radicals and the sulfur-hydrogen bond strength in mercaptans. *J. Am. Chem. Soc.* **1980,** *102*, 3125-9.